PROCEEDINGS OF SCIENCE

High-energy neutrino emission associated with gravitational-wave signals: effects of cocoon photons and constraints on late-time emission

Riki Matsui,[a,*] **Shigeo S. Kimura,**[a,b] **Kenji Toma**[a,b] **and Kohta Murase**[c,d,e]

[a] *Astronomical Institute, Graduate School of Science, Tohoku University, Sendai 980-8578, Japan*

[b] *Frontier Research Institute for Interdisciplinary Sciences, Tohoku University, Sendai 980-8578, Japan*

[c] *Department of Physics; Department of Astronomy and Astrophysics; Center for Multimessenger Astrophysics, Institute for Gravitation and the Cosmos, The Pennsylvania State University, University Park, Pennsylvania 16802, USA*

[d] *School of Natural Sciences, Institute for Advanced Study, USA*

[e] *Center for Gravitational Physics and Quantum Information, Yukawa Institute for Theoretical Physics, Kyoto University Kyoto, Kyoto 606-8502, Japan*

E-mail: riki.matsui@astr.tohoku.ac.jp

GW170817 and electromagnetic follow-up observations showed that binary neutron star mergers are accompanied by short gamma-ray bursts (sGRBs) and kilonovae.The former and the latter are produced by jets and ejecta from neutron stars. sGRBs have extended emission components lasting 100-1000 s, whose emission mechanism is under debate. The jet emissions produced by prolonged central engine activity could explain the components. The jet should propagate inside the ejecta, forming a cocoon around the jet. Photons filled in the cocoon should diffuse into the dissipation region of the jet. We calculate the neutrino emission from the jet due to prolonged engine activity, taking into account the interaction between cocoon photons and cosmic rays accelerated in jets. We find that the detection of neutrino signals associated with gravitational waves is achieved with a high probability for 10 years of operation by the future project, IceCube-Gen2, and the second-generation gravitational wave detectors. Otherwise, we can put meaningful constraints on dissipation radius and baryon loading factor.

38th International Cosmic Ray Conference (ICRC2023)
26 July - 3 August, 2023
Nagoya, Japan

*Speaker

PoS(ICRC2023)1497

1. Introduction

The gravitational-wave signal, GW170817, and electromagnetic follow-up observations showed that binary neutron star mergers are accompanied by short gamma-ray bursts (SGRBs) and kilonovae [e.g. 3, 16]. The former and the latter are produced by jets and ejecta from neutron stars.

SGRBs, a prominent target of multi-messenger astronomy, have an extended emission component that lasts 100-1000 s after prompt emission [e.g. 18], but the emission mechanism of the component is under debate. The most plausible scenario is the internal dissipation of the jet produced by the activity of the central engine at a late time [11]. To confirm the mechanism, we need to carefully study the properties of the emission component, such as the dissipation radius, Lorentz factor, and so on.

The high-energy neutrino is thought to be a powerful prove to investigate the jet of gamma-ray bursts (GRBS). IceCube [1] is now the most sensitive detector for high-energy neutrinos. Furthermore, future detectors, such as IceCube-Gen2 [2], KM3Net/ACRA [5], baikal-GVD [6], P-One [4], and TRIDENT [20], will significantly increase neutrino detections. [13] evaluated the detectability of the neutrino associated with extended emission. However, the calculations in previous work do not take into account the external photon field produced by the materials around the jet. The jet should propagate inside the ejecta, forming a cocoon around the jet. Photons filled in the cocoon should diffuse into the dissipation region of the jet, and they can interact with protons in the jet to produce neutrinos. Therefore, in this work, we calculate the neutrino emission from the jet due to prolonged engine activity, taking into account the interaction between cocoon photons and cosmic rays accelerated in jets.

2. Neutrino Production and Cocoon Photons

The main process for producing high-energy neutrinos in GRBs is the photomeson pion production process and pion decay. In this section, we formulate the neutrino fluence measured on the earth, and introduce the method of the calculation as shown in [15].

2.1 Formulation

The neutrino spectrum produced by the photomeson process is approximately given by

$$\frac{dN_{\nu_\mu}}{d\varepsilon_{\nu_\mu}} \approx \int d\varepsilon_\pi g(\varepsilon_\pi, \varepsilon_{\nu_\mu}) f_{\mathrm{sup},\pi} \left(f_{p\gamma} \frac{dN_p}{d\varepsilon_p} \right) \Bigg|_{\varepsilon_p = 5\varepsilon_\pi} \tag{1}$$

for muon neutrinos, and

$$\frac{dN_{\bar{\nu}_\mu}}{d\varepsilon_{\bar{\nu}_\mu}} \approx \frac{dN_{\nu_e}}{d\varepsilon_{\nu_e}} \approx \int d\varepsilon_\mu g(\varepsilon_\mu, \varepsilon_{\nu_e}) f_{\mathrm{sup},\mu} \left(f_{\mathrm{sup},\pi} f_{p\gamma} \frac{dN_p}{d\varepsilon_p} \right) \Bigg|_{\varepsilon_p = 5\varepsilon_\pi = \frac{20}{3}\varepsilon_\mu} \tag{2}$$

for anti-muon neutrinos and electron neutrinos, where $f_{p\gamma}$, $f_{\mathrm{sup},i}$ (i = π, or μ), $g(\varepsilon_i, \varepsilon_j)d\varepsilon_j$, ε_i (i = p, π, or μ), and $dN_p/d\varepsilon_p$ are the pion production efficiency by photomeson production, the suppression factor by the pion and muon coolings, the distribution function of the secondary particle j produced by the decay of the parent particle i of energy ε_i, energy of a particle, and differential number of protons in the engine-rest frame, respectively. The production efficiency is given by $f_{p\gamma} = t'_{\mathrm{cool}}/t'_{p\gamma}$,

where $t'_{\rm cool}$ is the total cooling timescale of protons. We define $t'_{\rm cool} = (t'^{-1}_{\rm ad} + t'^{-1}_{\rm BH} + t'^{-1}_{p\gamma} + t'^{-1}_{\rm p,syn})^{-1}$, where each term represents adiabatic cooling, Bethe-Heitler process, photomeson production, and synchrotron cooling, respectively.

The suppression factor is determined by $f_{{\rm sup},i} = 1 - \exp(-t'_{i,\rm cool}/t'_{i,\rm dec})$ ($i = \pi$, or μ), where $t'_{i,\rm dec}$ and $t'_{i,\rm cool}$ are the lifetime and the cooling timescale of each particle in the comoving frame of the jet, respectively. The lifetime is given by $t'_{i,\rm dec} = t_i \varepsilon'_i/(m_i c^2)$, where t_i is the lifetime in the particle rest frame, and m_i is the mass of a particle. $t'_{i,\rm cool}$ is estimated to be $t'^{-1}_{i,\rm cool} = t'^{-1}_{i,\rm syn} + t'^{-1}_{\rm ad}$,

We approximate $g(\varepsilon_\pi, \varepsilon_{\nu_\mu}) = 4\Theta(\varepsilon_\pi - 4\varepsilon_{\nu_\mu})/\varepsilon_\pi$ and $g(\varepsilon_\mu, \varepsilon_{\nu_e}) = 3\Theta(\varepsilon_\mu - 3\varepsilon_{\nu_e})/\varepsilon_\mu$, where $\Theta(x)$ is Heaviside step function, since they imitate secondary distributions for the two-body decay. This treatment can approximately explain the low-energy tail of the neutrino spectrum, which would affect the detectability of neutrinos. Here, we assume that all pions produced by the photomeson production with ε_p have $\varepsilon_\pi = 0.2\varepsilon_p$, and all muons produced by the decay of pions with ε_π have $\varepsilon_\mu = (3/4)\varepsilon_\pi$.

2.2 Timescale for each particles and the photon distribution

The adiabatic and synchrotron cooling timescales are calculated by $t'_{\rm ad} = r_{\rm diss}/(\Gamma_j c)$ and $t'_{i,\rm syn} = 6\pi m_i^4 c^3/m_{\rm e}^2 \sigma_T B'^2 \varepsilon'_i$ (i = p, π, or μ), respectively, where $r_{\rm diss}$, Γ_j,c, m_i, m_e, σ_T, and B' are the dissipation radius, the Lorentz factor of the jet, the speed of light, mass of a particle, the electron mass, the Thomson cross section, and the magnetic field strength of the dissipation region in the comoving frame of the jet, respectively. The magnetic field is given by $B' = \sqrt{(2L_{\gamma,\rm iso}\xi_B)/(c\Gamma_j^2 r_{\rm diss}^2)}$, where $L_{\gamma,\rm iso}$ and ξ_B is the isotropic-equivalent luminosity of extended emission and a phenomenological parameter.

The cooling rates (the inverse of timescale) for Bethe-Heitler and photomeson production processes are estimated to be

$$t'^{-1}_{p\gamma/\rm BH} = \frac{c}{2\gamma'^2_p} \int_{\bar{\varepsilon}_{\rm th}}^{\infty} d\bar{\varepsilon}_\gamma \sigma(\bar{\varepsilon}_\gamma)\kappa(\bar{\varepsilon}_\gamma)\bar{\varepsilon}_\gamma \int_{\bar{\varepsilon}_\gamma/2\gamma_p}^{\infty} d\varepsilon'_\gamma \varepsilon'^{-2}_\gamma \frac{dn'_\gamma}{d\varepsilon'_\gamma}, \tag{3}$$

where $\bar{\varepsilon}_{\rm th}$, $\sigma(\bar{\varepsilon}_\gamma)$, $\kappa(\bar{\varepsilon}_\gamma)$, $\gamma'_p = \varepsilon'_{\rm p}/(m_{\rm p}c^2)$, ε'_γ, and $dn'_\gamma/d\varepsilon'_\gamma$ are the threshold energy, the cross-section, inelasticity for each reaction in the proton rest frame, the Lorentz factor of protons, the photon energy, and differential number density of photons, respectively. For the cross section and inelasticity of photomeson production, we use the fitting formulae based on GEANT4 for [17]. For the Bethe-Heitler process, we use the analytical fitting formulas given in [8, 19]. We define $t_{p\gamma,\rm int}$, $t_{\rm BH,int}$, $t_{p\gamma,\rm coc}$, and $t_{\rm BH,coc}$ as the cooling timescales using the internal photons and the cocoon photons for two processes, respectively.

We consider two component of the photon field in the dissipation region of the jet. One is the external photons entering into the dissipation region from the cocoon (hereafter, cocoon photons) and the other is the internal photons observed as extended emission of the sGRB (hereafter, internal photons). We modeled the spectrum of the cocoon photons as

$$\varepsilon'_\gamma \frac{dn'^{\rm coc}}{d\varepsilon'_\gamma} = \Gamma_j \frac{8\pi(\varepsilon'_\gamma/\Gamma_j)^3}{h^3c^3} \frac{1}{\exp[\varepsilon'_\gamma/(\Gamma_j k_B T_{\rm coc})] - 1} \times e^{-\tau}, \tag{4}$$

where h, k_B, $T_{\rm coc}$, and τ are the Planck constant, the Boltzmann constant the cocoon temperature, the lateral optical depth of the jet, respectively. The cocoon temperature is caluculated by

Table 1: fiducial parameters

Parameters	Γ_j	$t_{\rm dur}$ (s)	$L_{\rm X,iso}$ (erg/s)	$r_{\rm diss}$ (cm)	$\varepsilon_{\gamma,\rm pk}$ (keV)	$\varepsilon_{\gamma,\rm min}$ (keV)	$\varepsilon_{\rm X,min}$, $\varepsilon_{\rm X,max}$ (keV)
	200	$10^{2.5}$	10^{48}	10^{12}	10	10^{-4} , 10^{3}	0.3 , 10 (XRT)
	α	β	$p_{\rm inj}$	ξ_p	ϵ_p	ξ_B	d_L (Mpc)
	−0.5	−2	2.0	10	0.33	0.33	300

$T_{\rm coc} = [3\mathcal{E}_{\rm coc}/(4\pi R_{\rm coc}^3 a_{\rm rad})]^{1/4}$, where $R_{\rm coc} = 3.0\times10^{12}\, t_{\rm dur,2.5}$ cm, $a_{\rm rad}$, and $\mathcal{E}_{\rm coc}$ are the cocoon radius, the radiation constant, and the thermal energy of the cocoon, respectively. $\mathcal{E}_{\rm coc}$ is defined by $\mathcal{E}_{\rm coc} = \mathcal{E}_{\rm adi} + \mathcal{E}_{\rm rad}$, where $\mathcal{E}_{\rm adi} = 8.8\times10^{44} t_{\rm dur,2.5}^{-1}$ erg and $\mathcal{E}_{\rm rad} = 9.3\times10^{44}\, t_{\rm dur,2.5}^{-0.3}$ erg are the contributions of the initial thermal energy of the ejecta and by the radioactive decay of neutron-rich nuclei in the ejecta, as discussed in [12]. The optical depth is estimated to be $\tau = (L_{k,\rm iso}\sigma_T\theta_j)/(4\pi r_{\rm diss}\Gamma_j^2 m_p c^3)$, where θ_j and $L_{k,\rm iso}$ are the opening angle of the jet and the isotropic-equivalent kinetic luminosity, respectively. $L_{k,\rm iso}$ is estimated to be $L_{k,\rm iso} = L_{p,\rm iso}/\epsilon_p = \xi_p L_{\gamma,\rm iso}/\epsilon_p = 30\ (\xi_p/10)(\epsilon_p/0.33)^{-1} L_{\gamma,\rm iso}$, where $L_{p,\rm iso}$ is the luminosity of the accelerated protons, and ξ_p and ϵ_p are phenomenological parameters.

We assume $dn'_\gamma/d\epsilon'_\gamma$ for internal photons followed Band function:

$$\frac{dn'^{\rm in}}{d\varepsilon'_\gamma} = n_{\varepsilon'_\gamma,\rm nor} \begin{cases} \varepsilon_\gamma'^{\alpha} \exp\left(-\frac{(2+\alpha)\varepsilon'_\gamma}{\varepsilon'_{\gamma,\rm pk}}\right) & (\varepsilon'_\gamma \le \chi\varepsilon'_{\gamma,\rm pk}) \\ \varepsilon_\gamma'^{\beta}\ (\chi\varepsilon'_{\gamma,\rm pk}/e)^{\alpha-\beta} & (\varepsilon'_\gamma > \chi\varepsilon'_{\gamma,\rm pk}) \end{cases}, \tag{5}$$

where α, β, and $\chi = (\alpha-\beta)/(2+\alpha)$ are constants, and $n_{\varepsilon'_\gamma,\rm nor}$ and $\varepsilon'_{\gamma,\rm pk}$ are the normalization factor and the spectral peak energy in the jet comoving frame, respectively. The normalization factor is determined so that $L_{\rm X,iso} = 4\pi\Gamma_j^2 r_{\rm diss}^2 c \int_{\varepsilon_{\rm X,min}/\Gamma_j}^{\varepsilon_{\rm X,Max}/\Gamma_j} d\varepsilon'_\gamma \varepsilon'_\gamma (dn'_\gamma/d\varepsilon'_\gamma)$ is satisfied, where $L_{X,\rm iso}$ is the isotropic-equivalent luminosity in the X-ray band, and $\varepsilon_{\rm X,Max}$ and $\varepsilon_{\rm X,min}$ are the maximum and minimum energies of the X-ray band, respectively. Also, we can obtain $L_{\gamma,\rm iso} = 4\pi\Gamma_j^2 r_{\rm diss}^2 c \int_{\varepsilon'_{\gamma,\rm min}}^{\varepsilon'_{\gamma,\rm Max}} d\varepsilon'_\gamma \varepsilon'_\gamma (dn'_\gamma/d\varepsilon'_\gamma)$, where $\varepsilon'_{\gamma,\rm min}$ and $\varepsilon'_{\gamma,\rm max}$ are the minimum and maximum photon energies, respectively.

Figure 1 shows the timescales for protons as a function of the proton energy in the comoving frame of the jet for the fiducial parameter indicated by Table 1, and the timescales are explained by simple estimations. The most efficient process is the adiabatic cooling and photomeson production processes for $\varepsilon'_p \lesssim 10^4$ GeV and $\varepsilon'_p \gtrsim 10^4$ GeV, respectively. This critical energy, 10^4 GeV, for the photomeson production timescale corresponds to the threshold of the process. The critical energy is estimated to be $\tilde{\varepsilon}'_p \approx (\bar{\varepsilon}_{\rm th} m_p c^2)/\bar{\varepsilon}'_\gamma$, where $\bar{\varepsilon}'_\gamma$ is the typical photon energy in the comoving frame of the jet. As shown in Figure 1, $t'^{-1}_{p\gamma} \approx t'^{-1}_{p\gamma,\rm coc} \gg t'^{-1}_{p\gamma,\rm int}$ indicates $\bar{\varepsilon}'_\gamma = k_B T_{\rm coc}$ and $\tilde{\varepsilon}'_p \approx 1.3\times10^4\ (\bar{\varepsilon}_{\rm th}/0.1\ {\rm GeV})({\rm k_B T_{coc}}/20\ {\rm eV})^{-1}(\Gamma_{\rm j}/200)^{-1}$ GeV. We can also roughly estimate $t'^{-1}_{p\gamma,\rm coc} \approx n'_\gamma \sigma_{\rm eff} c$, where $\sigma_{\rm eff}$ is the peak effective cross section of the photomeson process. Substituting $n'_\gamma \approx (a_{\rm rad} T_{\rm coc}^3 \Gamma_j)/k_B$ gives $t'^{-1}_{p\gamma,\rm coc} \approx 88\ (\sigma_{\rm eff}/6\times10^{-29}\ {\rm cm^2})({\rm k_B T_{coc}}/20\ {\rm eV})^3(\Gamma_{\rm j}/200)\ {\rm s^{-1}}$. These values are consistent with the Figure 1.

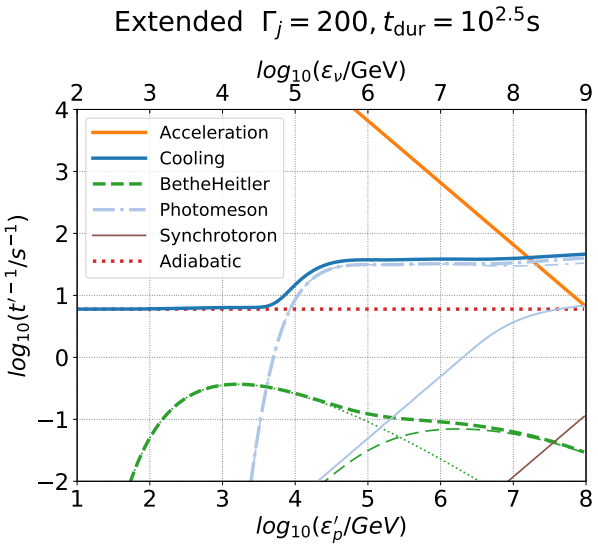

Figure 1: Acceleration and cooling rates for protons at the dissipation region in the comoving frame of the jet with various parameter sets (cited from [15]). The thick orange and thick blue lines represent the acceleration timescales and total cooling timescales, respectively. The red thick-dotted, the lightblue-thick-dot-dashed, and the green-thick-dashed lines represent $t'^{-1}_{\rm ad}$, $t'^{-1}_{p\gamma}$, and $t'^{-1}_{\rm BH}$, respectively. The lightblue-thin-solid and the lightblue-thin-dot-dashed lines represent $t'^{-1}_{p\gamma,{\rm int}}$ and $t'^{-1}_{p\gamma,{\rm coc}}$, respectively. The green-thin-dashed and the green-thin-dotted lines represent $t'^{-1}_{\rm BH,int}$ and $t'^{-1}_{\rm BH,coc}$, respectively.

2.3 Proton distribution and Neutrino spectra

We represent the differential number of protons in the engine-rest frame as

$$\frac{dN_p}{d\varepsilon_p} = N_{\varepsilon_p,{\rm nor}} \left(\frac{\varepsilon_p}{\varepsilon_{p,{\rm cut}}}\right)^{-p_{\rm inj}} \exp\left(-\frac{\varepsilon_p}{\varepsilon_{p,{\rm cut}}}\right), \tag{6}$$

where $\varepsilon_{p,{\rm cut}}$ and $N_{\varepsilon_p,{\rm nor}}$ is the normalization factor and the proton cutoff energy, respectively. $N_{\varepsilon_p,{\rm nor}}$ is determined by $L_{p,{\rm iso}} t_{\rm dur} = \xi_p L_{\gamma,{\rm iso}} t_{\rm dur} = \int_{\varepsilon_{\rm min}}^{\infty} d\varepsilon_p \varepsilon_p (dN_p/d\varepsilon_p)$, where ξ_p is the cosmic-ray loading parameter [17]. We use $\varepsilon_{p,{\rm min}} = \Gamma_j \varepsilon'_{\rm min} = 3\Gamma_j m_p c^2$ as the minimum energy of cosmic-ray protons. The cutoff energy is determined by the balance between the acceleration and cooling timescales : $t'^{-1}_{\rm acc}(\varepsilon_{p,{\rm cut}}) = t'^{-1}_{\rm cool}(\varepsilon_{p,{\rm cut}})$. We define the acceleration timescale as $t'_{\rm acc} = \varepsilon'_p/(ceB')$, where e is the elementary charge. $t'_{\rm acc}$ is also shown in Figure 1, and we get $\varepsilon'_{p,{\rm cut}} \sim 1.0 \times 10^7\ (\Gamma_j/200)^{-2}(B'/10^5{\rm G})$ GeV, considering $t'^{-1}_{p\gamma}$ is almost constant for $\varepsilon'_p \gtrsim 10^4$ GeV.

We can calculate $dN_\nu/d\varepsilon_\nu$ by using Eq.1 ∼ Eq.6, $f_{{\rm sup},i}$, and $g(\varepsilon_i, \varepsilon_j)d\varepsilon_j$ mentioned in 2.1. Taking into account the neutrino mixing [e.g., 7], the neutrino fluences measured on the earth are approximately given by

$$\phi_{\nu_\mu+\bar\nu_\mu} \approx \frac{4}{18}\phi^0_{\nu_e+\bar\nu_e} + \frac{7}{18}(\phi^0_{\nu_\mu+\bar\nu_\mu} + \phi^0_{\nu_\tau+\bar\nu_\tau}), \tag{7}$$

where $\phi^0_i = (dN_i/d\varepsilon_i)/(4\pi d_L^2)$ is the neutrino fluence measured on the Earth assuming that the flavor ratio is fixed at the source, and d_L is the luminosity distance.

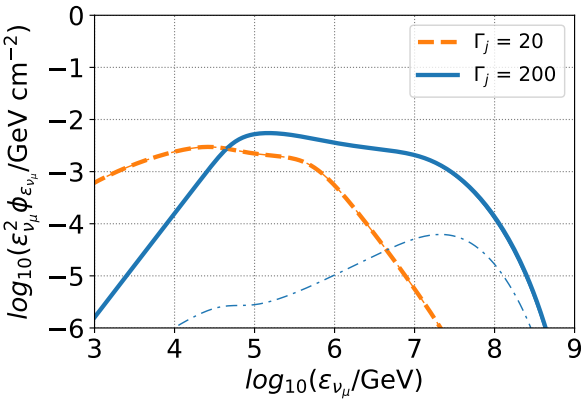

Figure 2: Neutrino fluences at the Earth (cited from [15]). The blue lines are for our fiducial parameter set, while the orange lines are for $\Gamma_j = 20$. The blue-thin-dot-dashed line is the contribution by the internal photons.

Figure 2 (blue line) shows $\phi_{\nu_\mu+\bar{\nu}_\mu}(\varepsilon_{\nu_\mu})$ for the fiducial parameters as Table 1 and the shape of the spectrum is explained by following discussions. The neutrino fluence are approximately written as $\varepsilon_\nu^2(d\phi_\nu/d\varepsilon_\nu) \propto f_{p\gamma} \times \varepsilon_p^2(dN_p/d\varepsilon_p)$. We have $f_{p\gamma} = 1 = \text{const.}$ for $\varepsilon'_p > \tilde{\varepsilon}'_p \approx 10^4$ GeV and $\varepsilon_p^2(dN_p/d\varepsilon_p) \sim \text{const.}$ for $\varepsilon'_p < \varepsilon'_{p,\mathrm{cut}} \sim 10^7$ GeV. This leads to the neutrino spectra expected to be top-hat shaped for 10^5 GeV $< \varepsilon_\nu < 10^8$ GeV, considering $\varepsilon_\nu \sim (\varepsilon'_{p,\mathrm{cut}}\Gamma_j)/20 \sim 10\,\varepsilon'_{p,\mathrm{cut}}$. This shape can explain the spectra shown in Figure 2, although $f_{\mathrm{sup},i}$ and $g(\varepsilon_i, \varepsilon_j)d\varepsilon_j$ modify the detail.

3. Prospects for future observation

The expected number of ν_μ-induced events is estimated to be

$$\bar{N}_{\nu_\mu} = \int d\varepsilon_{\nu_\mu} \phi_{\nu_\mu+\bar{\nu}_\mu}(\varepsilon_{\nu_\mu}) A_{\mathrm{eff}}(\delta, \varepsilon_{\nu_\mu}), \tag{8}$$

where A_{eff} is the effective area for a detector and δ is declination angle. We use the 10-year point-source analysis of IceCube [10] for A_{eff}. We assume that the effective area of IceCube-Gen2 is 5 times larger than that of IceCube. The probability of detecting more than one neutrino is given by

$$p_{n\geq 1} = 1 - \exp(-\bar{N}_{\nu_\mu}). \tag{9}$$

This probability depends on parameters, such as δ and t_{dur}, and we calculate the probability averaged over the solid angle and duration by

$$P_{n\geq 1} = \int \frac{d\Omega}{4\pi} \int d(\log_{10} t_{\mathrm{dur}}) F(t_{\mathrm{dur}})\ p_{n\geq 1}(\delta, t_{\mathrm{dur}}), \tag{10}$$

where $F(t_{\mathrm{dur}})$ is the distribution of duration, considering isotropic distribution for δ.

We assume $F(t_{\mathrm{dur}})$ as lognormal distribution:

$$F(t_{\mathrm{dur}}) = \frac{dN_{t_{\mathrm{dur}}}}{d\log_{10}(t_{\mathrm{dur}})} = F_0 \exp\left(-\frac{(\log_{10}(t_{\mathrm{dur}}/t_{\mathrm{dur},0}))^2}{2\sigma^2_{\log_{10} t_{\mathrm{dur}}}}\right), \tag{11}$$

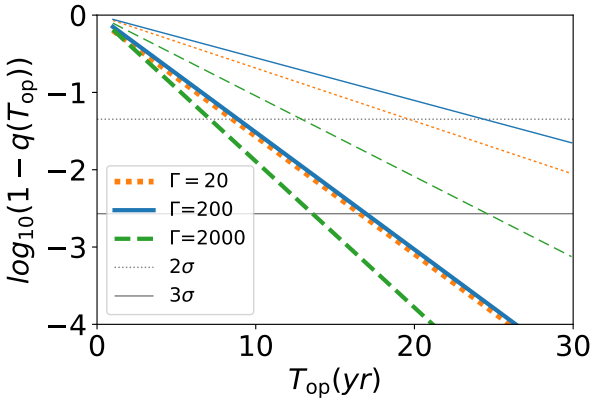

Figure 3: The probability of neutrino detection against the operation time (cited from [15]). The thin horizontal lines correspond to the significance of 2σ and 3σ. Thick and thin lines represent the models for IceCube and IceCube-Gen2, respectively. The dotted, solid, and dashed lines represent probability for $\Gamma_j = 20$, 200, and 2000, respectively.

where $t_{\rm dur,0}$ and $\sigma^2_{\log_{10}t_{\rm dur}}$ are the mean and variance of the duration, respectively. We fit the data of duration of observed extended emissions listed in [14] to obtain the values of $t_{\rm dur,0} = 10^{2.4}$ s and $\sigma^2_{\log_{10}t_{\rm dur}} = 8.3 \times 10^{-2}$.

We can estimate the probability of detecting more than one neutrino associated with GW signal in $T_{\rm op}$ (yr) to be

$$q(T_{\rm op}) = 1 - \exp\left(-T_{\rm op} R_{\rm sGRB} 4\pi \int^{300{\rm Mpc}} d(d_L) d_L^2 P_{n\geq 1}\right), \tag{12}$$

where $R_{\rm sGRB} = 8\ {\rm Gpc}^{-3}\ {\rm yr}^{-1}$ is the event rate of sGRB [e.g., 9]. Figure 3 (blue lines) represents the $q(T_{\rm op})$ for the fiducial parameters shown by Table 1. $q(T_{\rm op})$ achieves 0.955 (0.997), equivalent to 2σ (3σ) confidence level, within ∼10 (∼20) yr of observation with IceCube-Gen2. However, it takes longer than 20 yr by observation with IceCube.

4. Summary and Discussion

We found that the neutrino associated with the extended emission of sGRB and gravitational waves can be detected by IceCube-Gen2 in 10 years. However, we have uncertainty in the parameters of the jet produced by the late-time engine activity. The key parameters for neutrino emission are ξ_p and $r_{\rm diss}$. ξ_p is proportional to the neutrino fluence, but $r_{\rm diss}$ has a complex dependence on the fluence. For the smaller $r_{\rm diss}$, B' and $t'^{-1}_{\rm syn}$ increase, and the pion and muon synchrotron suppress neutrino emission. On the other hand, if $r_{\rm diss}$ is larger than $R_{\rm coc} = 3.0 \times 10^{12}\, t_{\rm dur,2.5}$, the cocoon photons cannot interact with protons in the dissipation region, which also suppresses neutrino emission. Future observations by IceCube-Gen2 will clarify the neutrino fluence of the extended emission, and the result may meaningfully constrain the parameter space of ξ_p and $r_{\rm diss}$.

Γ_j have played an important role in the neutrino emission from GRBs in the previous literature which only considered internal photons [e.g. 13, 21], but the results shown in Figure 3 have a weak dependence on Γ_j. In this paper, the cocoon photons make the neutrino production rate weakly

depend on Γ_j. For lower Γ_j, such as 20, $\tau > 1$ causes the cocoon photon to be shielded by the electron in the jet. In this case, only internal photons interact with protons, as was considered in the previous work. However, the maximum fluence for $\Gamma_j = 20$ is comparable to that for $\Gamma_j = 200$ as shown in Figure 2, resulting in almost the same $q(T_{\rm op})$ for $\Gamma_j = 20$ and $\Gamma_j = 200$ as in Figure 3.

References

[1] Aartsen, M. G., Abbasi, R., Abdou, Y., et al. 2013, PhRvL, 111, 021103, doi: 10.1103/PhysRevLett.111.021103

[2] Aartsen, M. G., Abbasi, R., Ackermann, M., et al. 2021, Journal of Physics G Nuclear Physics, 48, 060501, doi: 10.1088/1361-6471/abbd48

[3] Abbott, B. P., Abbott, R., Abbott, T. D., et al. 2017, ApJL, 848, L12, doi: 10.3847/2041-8213/aa91c9

[4] Agostini, M., Böhmer, M., Bosma, J., et al. 2020, Nature Astronomy, 4, 913, doi: 10.1038/s41550-020-1182-4

[5] Aiello, S., Akrame, S. E., Ameli, F., et al. 2019, Astroparticle Physics, 111, 100, doi: 10.1016/j.astropartphys.2019.04.002

[6] Avrorin, A. D., Avrorin, A. V., Aynutdinov, V. M., et al. 2014, Nuclear Instruments and Methods in Physics Research A, 742, 82, doi: 10.1016/j.nima.2013.10.064

[7] Becker, J. K. 2008, PhR, 458, 173, doi: 10.1016/j.physrep.2007.10.006

[8] Chodorowski, M. J., Zdziarski, A. A., & Sikora, M. 1992, ApJ, 400, 181, doi: 10.1086/171984

[9] Coward, D. M., Howell, E. J., Piran, T., et al. 2012, MNRAS, 425, 2668, doi: 10.1111/j.1365-2966.2012.21604.x

[10] IceCube Collaboration, Abbasi, R., Ackermann, M., et al. 2021, arXiv e-prints, arXiv:2101.09836. https://arxiv.org/abs/2101.09836

[11] Ioka, K., Kobayashi, S., & Zhang, B. 2005, ApJ, 631, 429, doi: 10.1086/432567

[12] Kimura, S. S., Murase, K., Ioka, K., et al. 2019, ApJL, 887, L16, doi: 10.3847/2041-8213/ab59e1

[13] Kimura, S. S., Murase, K., Mészáros, P., & Kiuchi, K. 2017, ApJL, 848, L4, doi: 10.3847/2041-8213/aa8d14

[14] Kisaka, S., Ioka, K., & Sakamoto, T. 2017, ApJ, 846, 142, doi: 10.3847/1538-4357/aa8775

[15] Matsui, R., Kimura, S. S., Toma, K., & Murase, K. 2023, ApJ, 950, 190, doi: 10.3847/1538-4357/acd004

[16] Mooley, K. P., Nakar, E., Hotokezaka, K., et al. 2018, Nature, 554, 207, doi: 10.1038/nature25452

[17] Murase, K., & Nagataki, S. 2006, PhRvD, 73, 063002, doi: 10.1103/PhysRevD.73.063002

[18] Norris, J. P., & Bonnell, J. T. 2006, ApJ, 643, 266, doi: 10.1086/502796

[19] Stepney, S., & Guilbert, P. W. 1983, MNRAS, 204, 1269, doi: 10.1093/mnras/204.4.1269

[20] Ye, Z. P., Hu, F., Tian, W., et al. 2022, arXiv e-prints, arXiv:2207.04519. https://arxiv.org/abs/2207.04519

[21] Zhang, B., & Kumar, P. 2013, PhRvL, 110, 121101, doi: 10.1103/PhysRevLett.110.121101